

# Experimental verification of the key properties of a three-dimensional isotropic transmission line based superlens

Pekka Alitalo, Stanislav Maslovski, and Sergei Tretyakov

*Radio Laboratory / SMARAD, Helsinki University of Technology*

*P.O. Box 3000, FI-02015 TKK, Finland*

E-mails: pekka.alitalo@tkk.fi, stanislav.maslovski@gmail.com, sergei.tretyakov@tkk.fi

(Dated: August 31, 2018)

## Abstract

Design and experimental realization of a three-dimensional superlens based on  $LC$ -loaded transmission lines are presented. Commercially available components and materials are used in the design. Transmission properties of the designed structure are studied experimentally and the observed lens properties are compared with analytical predictions. Backward-wave propagation and amplification of evanescent waves in the prototype structure are verified both analytically and experimentally.

## I. INTRODUCTION

Systems that are able to focus propagating electromagnetic waves and amplify evanescent waves have received a lot of attention after Pendry published his paper<sup>1</sup> about a superlens capable of subwavelength focusing. The amplification of evanescent waves is the key feature in the subwavelength focusing characteristics of the superlens, because evanescent waves carry information about fine details (smaller than the wavelength) of the source field. Pendry's superlens is based on a planar slab made of a backward-wave (BW) material (also called double-negative material or Veselago medium), in which the real parts of the effective permittivity and permeability are both negative.

The first successful demonstrations of a BW material and negative refraction were done using an array of resonant cells, which were comprised of thin wire strips (effective negative permittivity) and split-ring-resonators (effective negative permeability).<sup>3-5</sup> However, these structures are highly anisotropic and they allow one to achieve the properties of a BW material only within a narrow frequency band due to the use of resonant phenomena in split rings. Also, such systems would be very difficult to implement at RF-frequencies. This is why other ways to realize a BW material have been extensively studied in the recent literature. Another approach to create a BW material is based on *LC*-loaded transmission-line networks.<sup>6,7</sup> These networks do not rely on resonant response from particular inclusions, and the periods of the structures can be made very small as compared to the wavelength. These features allow realization of broadband and low-loss devices, which is extremely difficult if resonant inclusions are used.

So far the transmission-line (TL) network approach has been successfully realized in one- and two-dimensional networks,<sup>8,9</sup> and the main challenge on the route towards truly three-dimensional broadband and low-loss superlenses is the realization of isotropic three-dimensional artificial BW structures. In our recent paper we introduced a three-dimensional (3D) *LC*-loaded transmission-line network and derived necessary equations to design such a structure.<sup>10</sup> The key idea of our approach is that the inside volume of every TL section is effectively screened from the other sections and from the outer space.<sup>10</sup> Other ways to design three-dimensional FW and BW transmission-line structures have been proposed,<sup>11,12</sup> but to the best of our knowledge those structures have not been realized.

The goal of this paper is to show that the three-dimensional structure analytically de-

scribed earlier<sup>10</sup> can be practically manufactured and allows us to realize the two basic properties of Pendry’s superlens, i.e. backward-wave propagation and amplification of evanescent waves.

## II. THE DESIGNED STRUCTURE

The components that are used to realize the 3D superlens are listed in Table I with their main properties. The structure is designed to work at a frequency close to 1 GHz. The period of the structure ( $d$ ) should be much smaller than the wavelength ( $\lambda$ ) at this frequency. Accordingly, the period of the structure is chosen to be 13 mm ( $\lambda_0$  at 1 GHz is 300 mm,  $\lambda_0$  is the wavelength in free space). For the ease of manufacturing, the thickness of the BW slab ( $l$ ) has been decided to be three periods, i.e.  $l = 3d = 39$  mm. Using the equations for the characteristic impedances,<sup>10</sup> suitable impedance values of the TLs have been found to be  $Z_{0,TL,FW} = 66 \Omega$  (impedance of the TLs in the FW region) and  $Z_{0,TL,BW} = 89 \Omega$  (impedance of the TLs in the BW region). With these values the characteristic impedances of the FW and BW regions should be approximately equal. The height of the substrate is 0.787 mm (Rogers RT/Duroid 5870). The lumped elements, i.e., the capacitors and inductors, have been supplied by American Technical Ceramics Corp. (ATC).

TABLE I: Properties of the prototype components.

	Value	Tolerance	Manufacturer	Q-factor or loss tangent
$d$	13 mm	-	-	-
$Z_{0,TL,FW}$	66 $\Omega$	-	-	-
$Z_{0,TL,BW}$	89 $\Omega$	-	-	-
$C$	3.3 pF	$\pm 0.05$ pF	ATC	$Q_{C,1GHz} = 500$
$L$	6.8 nH	$\pm 0.136$ nH	ATC	$Q_{L,1GHz} = 50$
Substrate	$\epsilon_r = 2.33$	$\pm 0.02$	Rogers	$\tan \delta = 0.0012$

Using the well-known equations for microstrip lines, one can find the widths ( $w$ ) and the effective permittivities ( $\epsilon_{r,eff}$ ) for the required transmission lines (66  $\Omega$  and 89  $\Omega$ ). The results for the FW network are  $w_{FW} \approx 1.437$  mm,  $\epsilon_{r,eff,FW} \approx 1.902$ , and for the BW network  $w_{BW} \approx 0.794$  mm,  $\epsilon_{r,eff,BW} \approx 1.845$ .

Detailed description of the dispersion equations and characteristic impedances for the FW and BW networks will be published elsewhere<sup>10</sup> and due to their complexity they are not repeated here. By plotting the dispersion curves for the FW and BW networks, one can see that the matching frequency (at which the longitudinal component of the wavenumber in the BW region equals to the negative of the longitudinal component of the wavenumber in the FW region, i.e.  $k_{z,\text{BW}} = -k_{z,\text{FW}}$ ) is  $f \approx 0.8996$  GHz, see Fig. 1a. In the dispersion curves plotted here only propagation along the  $z$ -axis (lens axis) is considered. From Fig. 1a it is also seen that at the matching frequency the absolute value of  $k_z d$  is approximately 0.5909 (in both FW and BW regions), which corresponds to the longitudinal wavenumber  $k_z = 0.5909/d \approx 45.5 \text{ m}^{-1}$ . This is equal to the maximum transverse wavenumber ( $k_t$ ) that a propagating wave can have, and therefore we can conclude that for evanescent waves  $k_t > 45.5 \text{ m}^{-1}$ . The maximum transverse wavenumber for evanescent waves is at the edge of the first Brillouin zone:  $k_{t,\text{max}} = \pi/d \approx 242 \text{ m}^{-1}$ . By plotting the characteristic impedances ( $Z_0$ ) for the FW and BW networks, one can see that the characteristic impedances of the two networks are approximately equal at the design frequency ( $f \approx 0.8996$  GHz), see Fig. 1b.

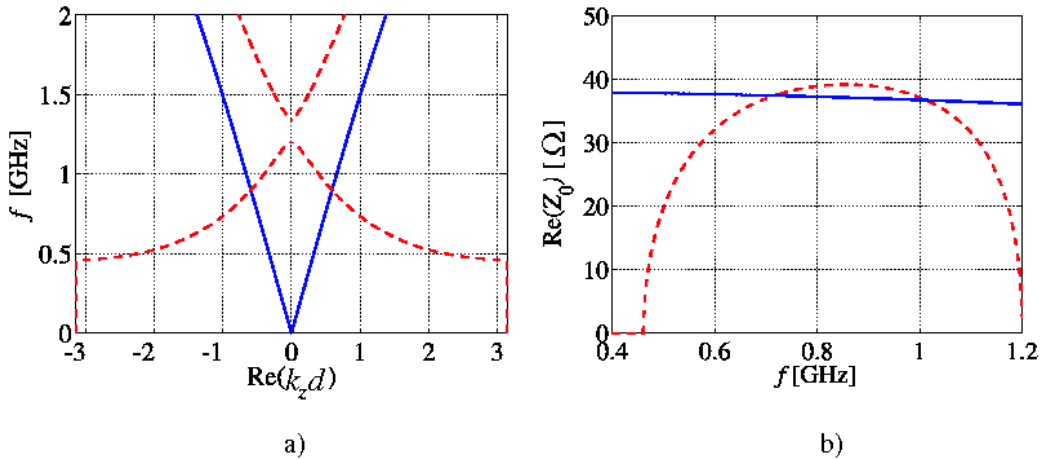


FIG. 1: a) Dispersion curves for the FW and BW networks (ideal, lossless components). b) Characteristic impedances for the FW and BW networks (ideal, lossless components). Propagation along the  $z$ -axis is considered. Solid lines: FW network, dashed lines: BW network.

### III. TRANSMISSION PROPERTIES OF THE DESIGNED STRUCTURE

The equation for the transmission coefficient of the lens ( $T_{\text{Lens}}$ ) as a function of the transverse wavenumber  $k_t$  was derived earlier<sup>10</sup>, and the result was:

$$T_{\text{Lens}}(k_t) = \frac{4Z_{0,\text{FW}}(k_t)Z_{0,\text{BW}}(k_t)}{[Z_{0,\text{FW}}(k_t) + Z_{0,\text{BW}}(k_t)]^2 e^{+jk_{z,\text{BW}}(k_t)l} - [Z_{0,\text{FW}}(k_t) - Z_{0,\text{BW}}(k_t)]^2 e^{-jk_{z,\text{BW}}(k_t)l}}, \quad (1)$$

where we again assume that the lens axis is parallel to the  $z$ -axis. The total transmission from the source plane to the image plane is then (the distance from the source plane to the lens is  $s_1$ , and the distance from the lens to the image plane is  $s_2$ )<sup>10</sup>

$$T_{\text{tot}}(k_t) = T_{\text{Lens}}(k_t) e^{-jk_{z,\text{FW}}(k_t) \cdot (s_1 + s_2)}. \quad (2)$$

To estimate the performance of the designed superlens, the total transmission from the source plane to the image plane can be plotted using equations (1) and (2), see Fig. 2a, where we have used  $s_1 = s_2 = 19.5$  mm and  $l = 39$  mm (lossless case).

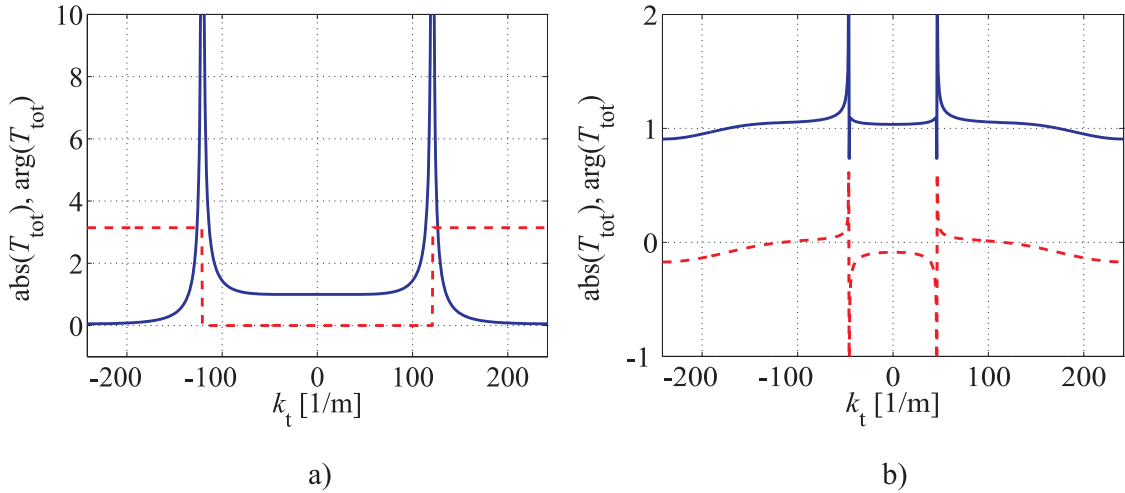


FIG. 2: Absolute value (solid line) and phase (dashed line) of the transmission coefficient of the designed superlens as a function of the transverse wavenumber. a)  $f = 0.8996$  GHz, ideal components. b)  $f = 0.91$  GHz, dissipation in the lumped components and in the substrate taken into account.

Tuning the frequency, imaging can be improved, effectively enhancing transmission of the modes with  $k_t > 45.5$  m<sup>-1</sup> (i.e., evanescent waves). This is due to a better matching of the characteristic impedances at those values of  $k_t$  that correspond to evanescent waves. For example, in the lossless case at  $f = 0.91$  GHz the transmission coefficient  $T_{\text{tot}}$  is practically

equal to unity for all transverse wavenumbers in the range  $0 \leq k_t \leq k_{t,\max}$ . The effect of dissipation caused by the substrate and the lumped components can be considered by taking into account the loss tangent ( $\tan \delta$ ) of the substrate and the quality factors ( $Q$ ) of the lumped components (shown in Table I), see Fig. 2b for this case. As is seen from Fig. 2b, the transmission properties of this lossy structure are close to the ideal case:  $|T_{\text{tot}}| \approx 1$  and  $\arg(T_{\text{tot}}) \approx 0$  for a wide range of  $k_t$  which includes propagating as well as evanescent spectral components.

#### IV. TWO-DIMENSIONAL PROTOTYPE

First, in order to check the operational principles of the proposed structure, a two-dimensional prototype was built (see Fig. 3). The prototype had the same properties and component values as shown in Table I. The edges of the structure were terminated with resistive loads that were approximately matched to the TL impedances. This was done in order to reduce reflections of the propagating modes from the edges of the structure.

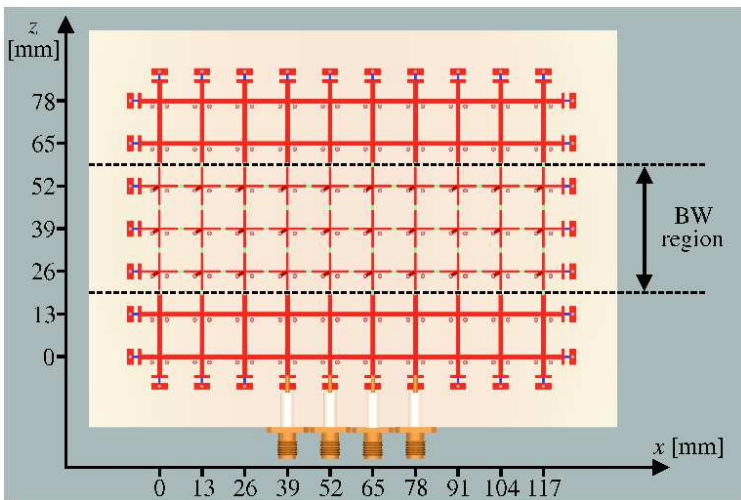


FIG. 3: (Color online). Two-dimensional prototype of the proposed structure (one horizontal layer of the designed 3D structure).

The structure was excited by a coaxial feed (SMA-connectors) connected to the edge of the first FW region as shown in the bottom of Fig. 3. To have a possibility to change the position of the excitation, four SMA-connectors were soldered to the structure. The inner conductors of the SMA-connectors were soldered to the microstrip lines and the outer

conductors to the ground. The SMA-connectors that were not used at each measurement were terminated with  $50 \Omega$  loads.

By connecting port 2 of a vector network analyzer to the excitation point(s) of the structure and port 1 to a probe antenna (a short vertical monopole antenna), the electric field distribution on top of the structure could be measured (by measuring  $S_{12}$ ). The measured vertical component of the electric field is proportional to the voltage at the network nodes, a non-invasive direct measurement of which can be a complicated task at 1 GHz. The probe antenna was connected to an automated measurement robot, which could be programmed to position the probe at certain points. Here the field was measured at the center of each node of the structure which corresponds to 70 measurement points. The BW region is situated in the area  $19.5 \text{ mm} < z < 58.5 \text{ mm}$ . See Fig. 4 for the measured electric field distributions on the top of the structure.

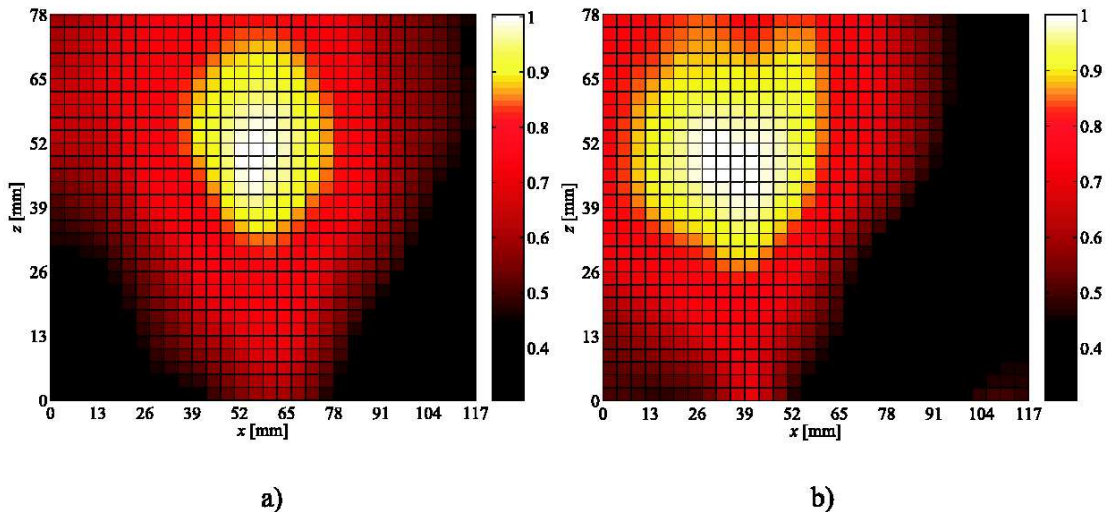


FIG. 4: (Color online). Measured amplitude of the vertical component of electric field on top of the 2D structure at  $f = 900 \text{ MHz}$ . Fields normalized to the maximum value. a) Symmetrical excitation by two sources at  $x = 52 \text{ mm}$ ,  $z = -6.5 \text{ mm}$  and  $x = 65 \text{ mm}$ ,  $z = -6.5 \text{ mm}$ . b) One source at  $x = 39 \text{ mm}$ ,  $z = -6.5 \text{ mm}$ .

As is seen in Fig. 4a and Fig. 4b, the maximum values of the amplitude occur at the back edge of the BW region (as it is expected from the theory). In Fig. 4b the point of excitation is displaced from the middle to show that the effects seen are not caused by reflections from the side edges. It is clear that both propagating and evanescent modes are excited in

the structure, because the fields do not experience significant decay in the first FW region (evanescent modes decay exponentially) and there is a remarkable growth of the amplitude in the BW region (only evanescent modes can be “amplified” in a passive structure like this). The experiment does not show any noticeable reflections at the FW/BW interfaces, which implies to a good impedance matching between the two types of networks.

To show that the structure supports backward waves, the time-harmonic electric field was plotted from the measured complex field using

$$E_{\text{real}} = \text{Re}\{E_{\text{complex}}e^{j\omega t}\}. \quad (3)$$

When the field plot is animated as a function of time, it is seen that the waves propagate “backwards” (towards the point of excitation) in the BW region. To illustrate this effect, some contour lines of the time-harmonic field are plotted in Fig. 5 with different values of the phase angle ( $\phi = \omega t$ ).

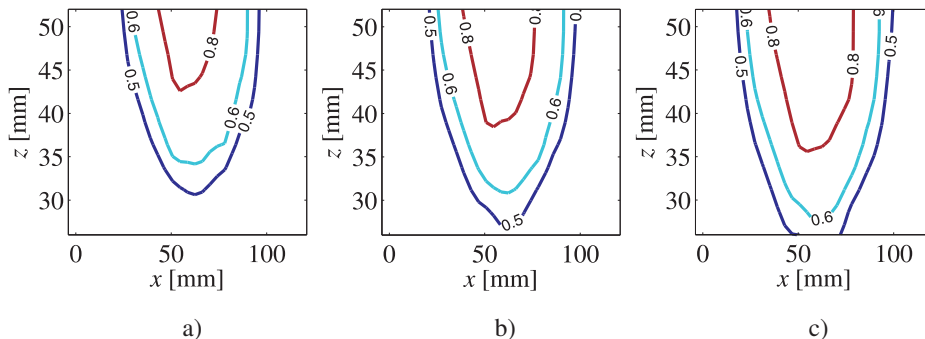


FIG. 5: (Color online). Time-harmonic electric field on top of the 2D structure at  $f = 900$  MHz. Fields normalized to the maximum value. Symmetrical excitation by two sources at  $x = 52$  mm,  $z = -6.5$  mm and  $x = 65$  mm,  $z = -6.5$  mm. a)  $\phi = 1$ , b)  $\phi = 1 + \pi/20$ , c)  $\phi = 1 + 2\pi/20$ .

## V. THREE-DIMENSIONAL REALIZATION

To realize a three-dimensional structure, a second two-dimensional layer as in section IV was manufactured. To connect these two layers, ten vertical sub-layers of height 12.2 mm were soldered between them. See Fig. 6a for the geometry of the structure (one horizontal layer and ten vertical sub-layers are shown). The resulting 3D structure is isotropic with respect to waves propagating inside the TLs (distance between adjacent horizontal and vertical



nodes remains the same and the vertical microstrip lines are also loaded with capacitors in the BW region). A photograph of the manufactured two-layer structure is shown in Fig. 6b.

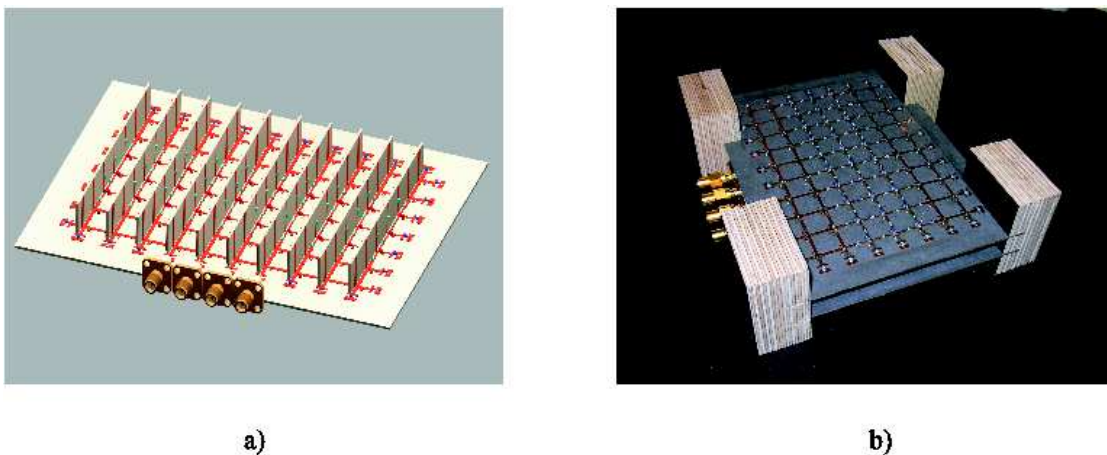


FIG. 6: (Color online). a) Geometry of the 3D structure (one horizontal layer and ten vertical sub-layers shown). b) Experimental prototype of the 3D structure with two horizontal layers.

Having more than one layer in the structure, wave propagation along the vertical axis (the  $y$ -axis) can be also experimentally tested. This was done by exciting the structure from the bottom of the lower horizontal layer at  $x = 78$  mm,  $z = 39$  mm. See Fig. 7 for the electric field distribution measured on top of the upper layer and Fig. 8 for the instantaneous electric field snapshots. Fig. 7 proves the three-dimensional isotropy of the proposed network that was predicted theoretically.<sup>10</sup> Fig. 8 demonstrates backward-wave propagation, because the point of the source appears to be a “sink” for moving contours of instantaneous values of the electric field.

Next, a third layer as in section IV was manufactured and appended to the top of the other two horizontal layers using vertical sub-layers as shown in Fig. 6a. A photograph of the manufactured three-layer structure is shown in Fig. 9. The structure was again excited using the same connectors as in section IV (situated now in the lowest horizontal layer). The electric field distribution on top of the upper layer was measured as in section IV. See Fig. 10 for the measured electric field distribution on the top of the structure.

As is seen in Fig. 10, the maximum field value occurs near the back edge of the BW region. Vertical propagation in the BW region was verified as in the case of two horizontal layers and similar results as in Fig. 7 and Fig. 8 were obtained.

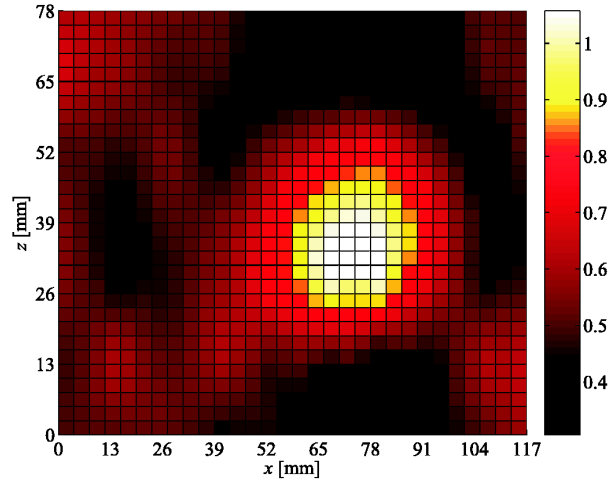


FIG. 7: (Color online). Measured amplitude of the vertical component of electric field on top of the 3D structure (two horizontal layers) at  $f = 900$  MHz. Fields normalized to the maximum value. One source below the lower horizontal layer at  $x = 78$  mm,  $z = 39$  mm.

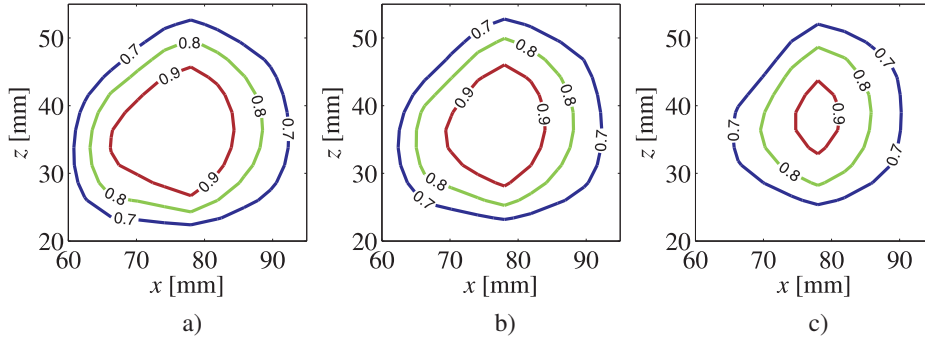


FIG. 8: (Color online). Time-harmonic electric field on top of the 3D structure (two horizontal layers) at  $f = 900$  MHz. Fields normalized to the maximum value. One source below the lower horizontal layer at  $x = 78$  mm,  $z = 39$  mm. a)  $\phi = 1.2$ , b)  $\phi = 1.2 + \pi/20$ , c)  $\phi = 1.2 + 2\pi/20$ .

## VI. CONCLUSIONS

In this paper we have described realization and testing of a three-dimensional transmission-line network which is a circuit analogy of the superlens proposed by Pendry. The backward-wave slab, which is the key part of this superlens, is implemented by loading a transmission-line network with lumped inductive and capacitive components. Detailed theoretical analysis of such structures will be published elsewhere.<sup>10</sup> In this paper we have shown

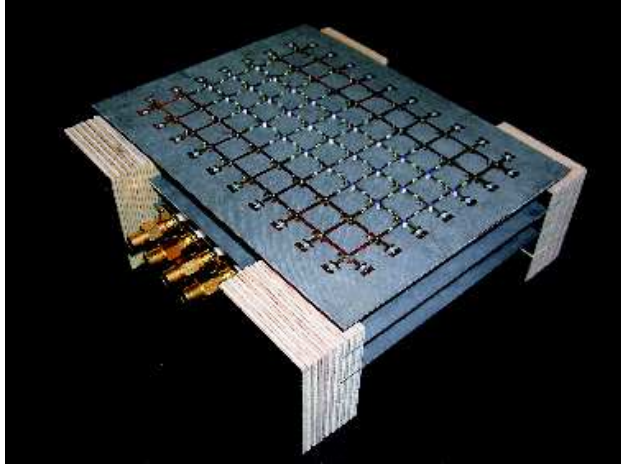


FIG. 9: (Color online). Experimental prototype of the 3D structure with three horizontal layers.

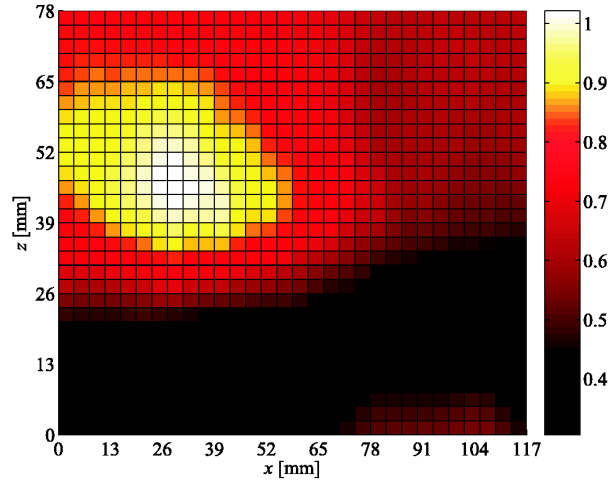


FIG. 10: (Color online). Measured amplitude of the vertical component of electric field on top of the 3D structure (three horizontal layers) at  $f = 900$  MHz. Fields normalized to the maximum value. One source at  $x = 39$  mm,  $z = -6.5$  mm, situated in the bottom layer.

that a realizable three-dimensional superlens can be quite easily designed and manufactured. A prototype of the designed structure has been built and backward-wave propagation and amplification of evanescent waves in the structure have been verified by measurements of electric field distributions.

## Acknowledgments

This work has been done within the frame of the *Metamorphose* Network of Excellence and partially funded by the Academy of Finland and TEKES through the Center-of-Excellence program. The authors would like to thank Dr. Mikhail Lapine for helpful discussions.

- 
- <sup>1</sup> J.B. Pendry, Physical Review Letters **85**, 3966 (2000).
  - <sup>2</sup> V.G. Veselago, Soviet Physics Uspekhi **10**, 509 (1968).
  - <sup>3</sup> D.R. Smith, W.J. Padilla, D.C. Vier, S.C. Nemat-Nasser, and S. Schultz, Physical Review Letters **84**, 4184 (2000).
  - <sup>4</sup> R.A. Shelby, D.R. Smith, and S. Schultz, Science **292**, 77 (2001).
  - <sup>5</sup> C.G. Parazzoli, R.B. Gregor, K. Li, B.E.C. Koltenbah, and M. Tanelian, Physical Review Letters **90**, 107401 (2003).
  - <sup>6</sup> G.V. Eleftheriades, A.K. Iyer, and P.C. Kremer, IEEE Trans. Microwave Theory and Techniques **50**, 2702 (2002).
  - <sup>7</sup> C. Caloz, H. Okabe, T. Iwai, and T. Itoh, Proc. USNC/URSI National Radio Science Meeting, San Antonio, USA **1**, 39 (2002).
  - <sup>8</sup> C. Caloz and T. Itoh, IEEE Trans. Antennas and Propagation, **52**, 1159 (2004).
  - <sup>9</sup> A. Grbic and G.V. Eleftheriades, Physical Review Letters, **92**, 117403 (2004).
  - <sup>10</sup> P. Alitalo, S. Maslovski and S. Tretyakov, “Three-dimensional isotropic perfect lens based on LC-loaded transmission lines,” arXiv:physics/0509149, submitted to Journal of Applied Physics (2005).
  - <sup>11</sup> A. Grbic and G.V. Eleftheriades, Journal of Applied Physics, **98**, 043106 (2005).
  - <sup>12</sup> W.J.R. Hofer, P.P.M. So, D. Thompson and M.M. Tentzeris, IEEE MTT-S International Symposium Digest, 313 (2005).